NANO LETTERS

pubs.acs.org/NanoLett Letter

At Least 10-fold Higher Lubricity of Molecularly Thin D_2O vs H_2O Films at Single-Layer Graphene–Mica Interfaces

Hu Lin, Lala Habibova, Abdul Rauf, José D. Cojal González, Nikolai Severin, Stefan Kirstein, Igor M. Sokolov, and Jürgen P. Rabe*

Cite This: *Nano Lett.* 2022, 22, 7761–7767 Read Online

ACCESS | Metrics & More | Article Recommendations | Supporting Information

ABSTRACT: Interfacial water is a widespread lubricant down to the nanometer scale. We investigate the lubricities of molecularly thin H_2O and D_2O films confined between mica and graphene, via the relaxation of initially applied strain in graphene employing Raman spectroscopy. Surprisingly, the D_2O films are at least 1 order of magnitude more lubricant than H_2O films, despite the similar bulk viscosities of the two liquids. We propose a mechanism based on the known selective permeation of protons vs deuterons through graphene. Permeated protons and left behind hydroxides may form ion pairs clamping across the graphene sheet and thereby hindering the graphene from sliding on the water layer. This explains the lower lubricity but also the hindering diffusivity of the water layer, which yields a high effective viscosity in accordance with findings in dewetting experiments. Our work elucidates an unexpected effect and provides clues to the behavior of graphene on hydrous surfaces.

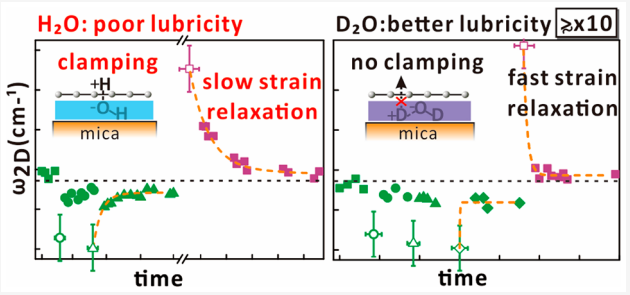

KEYWORDS: *water, shear, viscosity, proton permeation, filtering, tribology*

Solid friction and its reduction by a lubricant are topics of immense technological importance, and the phenomena are part of our everyday life. Interfacial water lubricates joints in our body, acts as lubricant in skating and skiing, and makes not only autumn leaves slippery but similarly also other layered materials like clays and graphite.[1,2] Graphite, for example, is a well-known solid lubricant, yet it is the ambient water that makes graphite lubricating under ambient conditions.[3] The underlying mechanisms of friction in systems of aromatic carbon materials and water remain debated.[4,5] To obtain a better understanding of lubrication, well-defined model systems are desirable.[6] An interface between 2D materials and mica is a powerful experimental system to investigate friction and lubricity on the scale of molecularly thin films. Mica is a layered mineral that can be easily cleaved, thereby producing atomically flat hydrophilic surfaces.[7] Therefore, it has been intensively used for investigating the rheology and the lubricity of liquids, squeezed down to molecularly thin films between two mica surfaces.[8] 2D materials exfoliated onto mica brought further experimental advantages into the field, since interfaces between mica and 2D sheets of choice can be filled with homogeneous and molecularly thin films of various molecules by exposing the samples to molecular vapors.[9,10] Straining the mica surface allows for transfer of the strain through the confined molecular film to the 2D sheets,[11,12] and the strained 2D sheets may then relax the strain with time (Figure 1A).[13] The comparison of strain relaxation in 2D sheets lying either directly on mica or on a molecular film confined between the sheet and mica allows assessing the lubricity of the films at the interface. The high sensitivity of the graphene Raman peak positions to strain renders graphene the 2D material of choice for such experiments.[14]

Here we want to gain a deeper understanding of the lubricity of a molecular water film at this model interface by comparing the properties of films of ordinary water (H_2O) with those of heavy water (D_2O). Most macroscopic physical properties of D_2O and H_2O are very similar. However, the difference in the isotopic composition of the molecules results in a difference of their vibrational frequencies, leading to differences in hydrogen bonding strengths and consequently in viscosities of bulk liquids. In bulk, D_2O is roughly 1.2 times more viscous than H_2O.[15] Therefore, one may expect a D_2O film to be less lubricating than an H_2O film. Contrary to this expectation, we find that the lubricity of a D_2O film on a mica–graphene is at least one order of magnitude higher than that of an H_2O film.

To prepare samples with either H_2O or D_2O films filling the graphene–mica interfaces, we start from initially dry samples

Received: April 8, 2022
Revised: September 1, 2022
Published: September 28, 2022

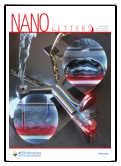

https://doi.org/10.1021/acs.nanolett.2c01425
Nano Lett. 2022, 22, 7761–7767

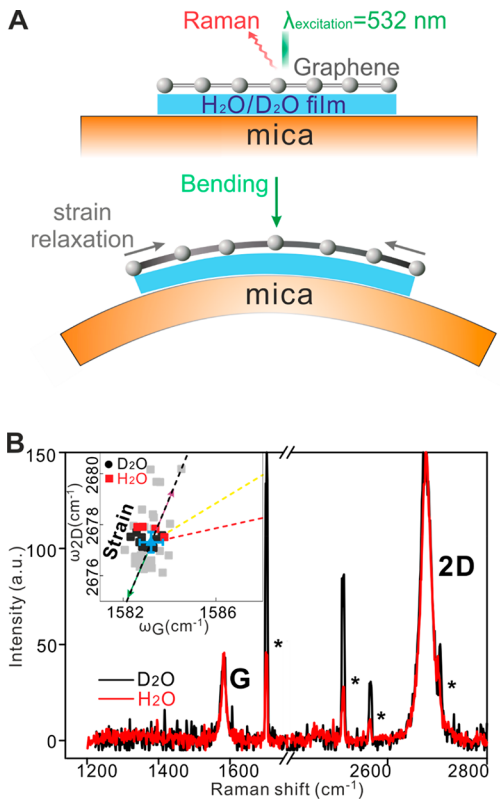

Figure 1. (A) Sketch of the setup (not-to-scale) used for the measurements of graphene strain relaxation. The mica slab was bent/unbent to strain/unstrain its outer surface. The subsequent time evolution of the strain in single-layer and bilayer graphene pieces was followed with Raman spectroscopy. The interfaces between graphene pieces and mica were filled with either H_2O or D_2O films. The simplified sketches do not show the molecular complexity of the H_2O/D_2O films hydrating the ionic mica surface.[20] (B) Typical Raman spectra recorded from single-layer graphene pieces lying on an unstrained mica surface. The samples were exposed to 40% RHs of H_2O (red curve) or D_2O (black curve) vapors, in order to fill the interfaces with the respective molecular films. The G and 2D peaks are labeled and the spectra are normalized to the 2D peak heights. The peaks labeled with asterisks (*) originate from a neon lamp and are used as calibration references. The inset shows 2D versus G peak positions recorded on graphene monolayers. The peak positions shown with red circles and black squares were recorded on graphene monolayers on H_2O and D_2O films, respectively, and on an unstrained mica surface. The cyan triangle shows the 2D and G peak positions reported for uncharged and unstrained graphene.[9] The gray squares are the peak positions recorded during strain relaxation in a graphene monolayer shown in Figure 2A. The black, yellow, and red dashed lines are the expected shifts induced by strain (slope 2.2), p-charge (slope 0.55) and n-charge (slope 0.2) doping of graphene, respectively.[16] The lines are guides for the eye.

and fill the graphene−mica interfaces with H_2O or D_2O films by exposing the samples to a mixture of nitrogen gas and the respective vapors at a given partial pressure. The samples were prepared in a glovebox filled with dry nitrogen, and the samples were not exposed to ambient before or during the measurements (see the Supporting Information). This procedure guarantees a high purity of the intercalating films. Figure 1B shows typical Raman spectra taken on single-layer graphene (SLG) on unbent mica after exposure of the initially dry samples to H_2O or D_2O vapors with relative humidity (RH) of 40%. Such RH is high enough to fill the graphene−mica interface with a uniform film of H_2O[9] and, as shown below, with a uniform film of D_2O as well. In in the following, we show and analyze the G and 2D peaks, since they are intense and their positions are rather sensitive to strain and charge doping of graphene.[14] For SLG on unbent mica, the spectra on H_2O and D_2O are nearly identical. Plotting the 2D vs the G peak positions (inset to Figure 1B) is an efficient way to quantify graphene strain and charge doping.[16] It was shown previously that SLGs exfoliated directly onto a mica surface are charged and strained, but filling the graphene−mica interface with a uniform H_2O film removes both the strain in graphene and its charge doping.[9,17] The 2D and G peak positions recorded for graphene pieces on D_2O (Figure 1B inset, peaks at 1583 ± 0.5 cm^{-1} and 2677.4 ± 0.3 cm^{-1}, respectively) imply that the graphene pieces on D_2O are practically uncharged and unstrained,[9] as is the case for H_2O. This is not astonishing, since most properties of D_2O and H_2O molecules, in particular their dipole moments, are rather similar,[18,19] and thus the D_2O film at the interface with the ionic mica surface should be structurally similar to the H_2O one.[20]

The vanishing strain in the samples filled by H_2O and by D_2O implies that both molecular films lubricate the interface.[13] To further investigate their lubricity, we study the kinetics of the strain relaxation. Thus, we bend the mica substrate to a given curvature, and measure than the strain of graphene as a function of time. In Figure 2, we plot the 2D peak positions as being more strain sensitive versus time.

Our key result is that the strain relaxation in SLGs on H_2O is at least an order of magnitude slower than the strain relaxation in SLGs on D_2O. The corresponding results are shown in Figure 2. The strain relaxation in graphene pieces on an H_2O film is exponential with a characteristic time of 8 ± 3 min (Figure 2A and Supporting Information).[13] The error margins here and in the following are standard deviations (SD) characterizing the data scattering. The relaxation on D_2O is fast, beyond the temporal resolution available in our experiments, and we can only provide the upper bounds of the corresponding characteristic times.

Within the simplest mechanical model, the kinetics of strain relaxation in the center of a graphene flake is exponential, $\varepsilon(t) \propto e^{-t/\tau}$, with the characteristic relaxation time τ depending on the flake's size[13] as $\tau \propto \frac{\alpha L^2}{Eh}$, where L is length of graphene along the strain direction, h is its thickness, E is the elastic modulus of graphene, and α is the viscous friction coefficient in units of force per unit area and per unit velocity. From the friction coefficient, a shear viscosity can be estimated[13] that corresponds to that of pitch.[22]

We measured 7 SLG pieces on H_2O. The characteristic time scale τ of strain relaxation is obtained by fitting the 2D peak positions at different times with a three-parametric exponential form

$$\omega_{2D}(t) = A\exp\left(-\frac{t - t_0}{\tau}\right) + B \quad (1)$$

where t_0 is the time at which mica was bent. Here $(A+B)$ is the initial 2D peak position at $t = t_0$, and B is the 2D peak position after full relaxation. The values of B imply that the strains in graphene did not converge to zero, but rather to a small average value of $0.03 \pm 0.02\%$, assuming $\Delta w_{2D}/\Delta\varepsilon = 64$ cm^{-1}/%. The reason for the strains not to converge to zero is not clear, yet the remaining strains are small compared with the

https://doi.org/10.1021/acs.nanolett.2c01425
Nano Lett. 2022, 22, 7761−7767

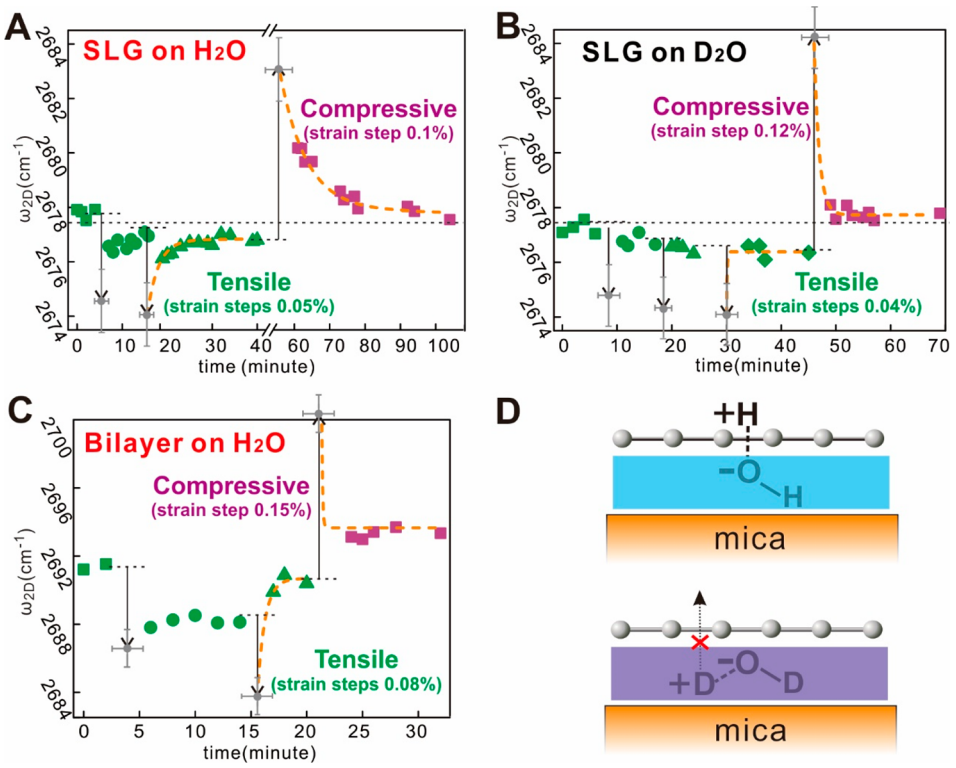

Figure 2. 2D peak position vs time for (A, B) single-layer and (C) bilayer graphene lying on (A, C) H_2O and (B) D_2O films. The mica slab was bent in a few steps (green symbols) and then unbent in one step (purple symbols). Open symbols show the expected 2D peak positions assuming the graphene strain to match the mica surface strain, and furthermore assuming $\Delta w_{2D}/\Delta\varepsilon$ = 64 cm^{-1}/% and $\Delta w_{2D}/\Delta\varepsilon$ = 64 cm^{-1}/% for single-layers and bilayers, respectively.[14,21] The orange dashed lines exemplify fits with exponential decay functions; in B and C, the lines correspond to an upper bound estimation for relaxation times (see discussion). The vertical arrows show the 2D peak shifts expected for graphene matching the mica surface strain. The horizontal error bars show the time uncertainties for the delay between straining of mica and recording of spectra. The vertical error bars are the sum of the uncertainties of mica surface strain estimation and of the scattering of peak positions due to limited precision of the Raman laser spot manual repositioning. The horizontal black dashed lines indicate the 2D peak position, expected for undoped and unstrained graphene (cyan triangle in Figure 1B). (D) Not-to-scale sketch of an (H+ OH−) ion pair proposed to clamp across graphene and hinder its sliding. The simplified sketches do not show the molecular complexity of the films hydrating the ionic mica surface.[20] Water molecules at the interface thermally dissociate into protons and hydroxides. The protons can permeate through graphene, forming a proton−hydroxide electrostatically bound (dashed line) ion pair with the bond across the graphene. Graphene is largely impermeable to deuterons, and thicker graphenes are impermeable to both protons and deuterons, thus clamping by the ion pairs should happen just for water at the single-layer graphene−mica interface.

strains induced by mica bending, and we do not discuss them in the following.

In three investigated SLG samples on D_2O, the Raman spectra acquired in less than 3 min after bending the mica substrate revealed that the flakes were already practically unstrained. Subsequently acquired spectra revealed no further change in strain (Figure 2B and Supporting Information). Thus, strain relaxation in the graphene pieces on D_2O happened within the time needed to restart the spectra acquisition and to acquire the first Raman spectrum. This implies that D_2O films exhibit substantially higher lubricity at the mica−SLG interface as compared with H_2O ones.

Mechanical exfoliation does not allow good control over the size and shape of the graphene pieces. To compare the lubricity of the D_2O and H_2O films, we selected graphene pieces of roughly the same size (the length of graphene pieces along the strain direction did not vary by more than a factor of 2). The average lengths of graphene pieces were 8 ± 3 μm and 6 ± 2 μm for D_2O and H_2O, respectively. That is, the size of SLG on D_2O was slightly larger, and thus one could expect slower strain relaxation, yet all three graphene pieces on D_2O relaxed much faster than the pieces on H_2O.

Nevertheless, we fitted all the strain vs time dependencies for D_2O with our eq 1, like we did for H_2O. For this, we assumed that there was an initial strain in graphene at the time t_0 matching the mica's surface strain difference induced by the bending steps. The characteristic relaxation time of SLG strain on D_2O was about 0.2 ± 0.3 min, which indicates an order of magnitude faster relaxation compared with graphene on H_2O. Possibly, however, strain relaxation in graphene pieces was even faster, i.e., it happened already during mica bending. Therefore, the fits provide only upper bounds of the relaxation times. Similar to H_2O, the fits revealed that the strains in graphene pieces did not relax to zero, the average residual frequency shift corresponded to 0.01 ± 0.01%.

As an additional check for the explanation of the poor H_2O lubricity under a graphene monolayer provided below, we investigated strain relaxation in bilayer graphenes (BLG) lying on a H_2O film. Two BLG pieces with a size of 7 ± 2 μm were investigated. Strain relaxation in both pieces was faster than our experimental time resolution. The fits gave characteristic times of 0.6 ± 0.3 min for the BLGs on H_2O. Thus, strain relaxation in BLGs on H_2O was also about an order of magnitude faster than in graphene monolayers.

https://doi.org/10.1021/acs.nanolett.2c01425
Nano Lett. 2022, 22, 7761−7767

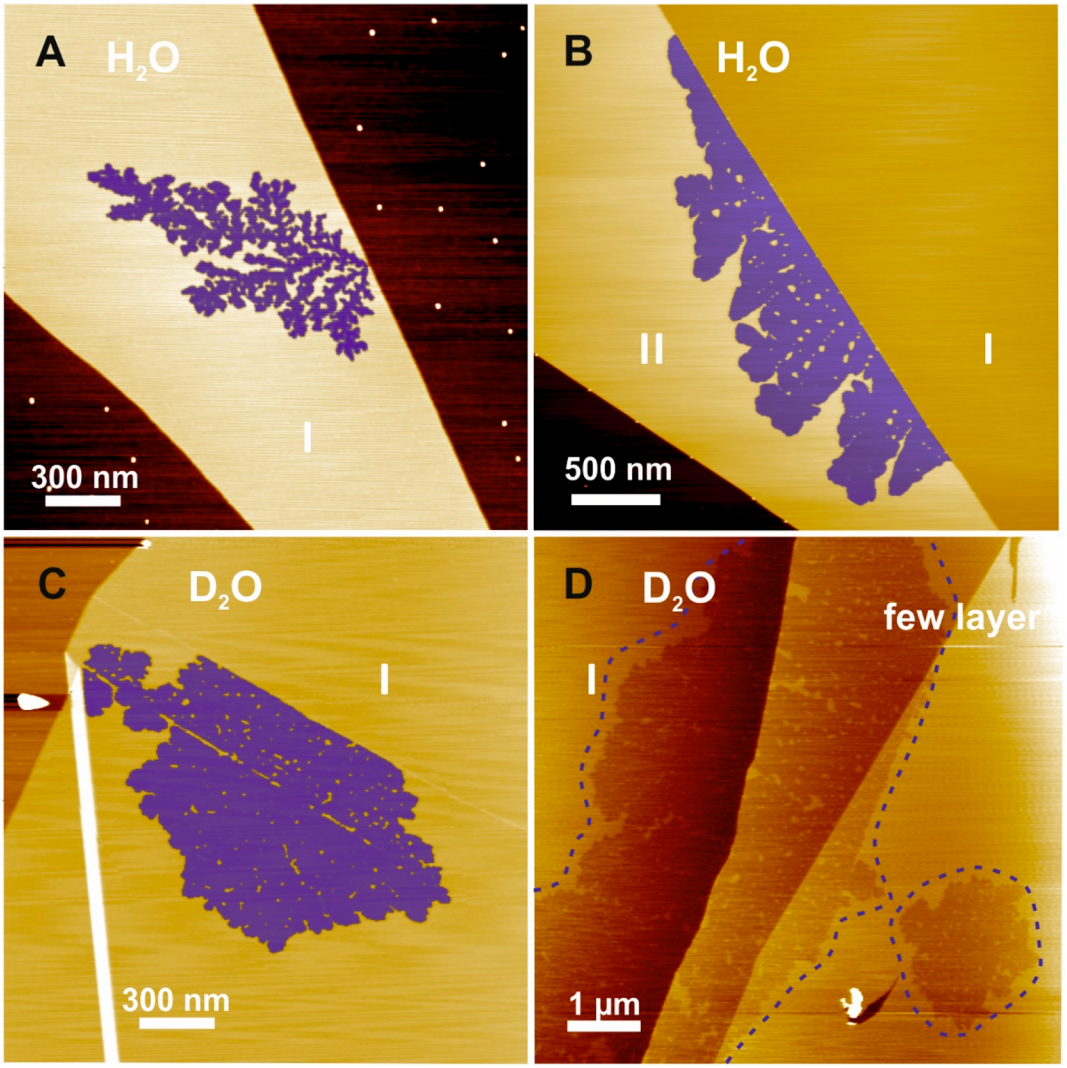

Figure 3. AFM topography images showing dewetting patterns of single-layer graphene on (A) H_2O and (B) D_2O, and (C)double-layer graphene on H_2O and (D) multilayer graphene on D_2O. Graphene monolayers and bilayer are indicated with **I** and **II**, respectively. The dewetting patterns are colored with blue color in A to C, and they are highlighted with blue dashed lines in D. The color is a guide for the eye, the uncolored images are shown in the Supporting Information with information on the depth of the dewetting patterns. The RH was decreased moderately ("slow dewetting", see text) from 40 to 13% within 2 min, and then it was kept constant in A–C. The growth of the dewetting patterns saturated on an hour time scale. In D, the RH was also decreased slowly from 26 to 4% within 15 min; then RH was decreased to 1% within 1 h. The H_2O dewetting patterns under graphene monolayer in A propagate in the shape of fractals with a fractal dimension of about 1.7. The shape of dewetting patterns in other cases is more compact with a fractal dimension around 1.85. We explain the fractal dewetting patterns under the graphene monolayer with a high effective viscosity of the H_2O film at the interface.

To obtain further insight into the difference between D_2O and H_2O lubricities, we filled the graphene–mica interface with mixtures of D_2O and H_2O. The strain relaxation in graphene for 30 and 70% of H_2O content showed the same behavior as pure D_2O and was faster than our experimental time resolution. Only for 90% of H_2O content could we detect a tail of a rather fast relaxation with a time constant of about 2 min in one of two graphene pieces (see the Supporting Information). This implies that the difference in lubricities between H_2O and D_2O could be even larger than an order of magnitude.

The giant difference in the strain relaxation kinetics on water and heavy water limited to graphene monolayers is rather surprising. The h-dependence of τ implies that graphene bilayers should relax strain two times faster than monolayers, assuming that the lubricity of the liquid films does not depend on the thickness of the cover. The contradiction of the implication with our results suggests that this assumption is wrong. We will propose a mechanism for this further below. Before, however, we discuss mechanisms that possibly contribute but cannot explain the anomalously poor lubricity of H_2O film confined at the graphene monolayer–mica interface.

For samples prepared and kept in a clean and dry environment (see the Supporting Information), we cannot expect the interfaces between graphene and mica to be significantly contaminated.[9,23] Nevertheless, we do not completely exclude any surface contamination of mica,[24,25] and thus of the interface, with organic molecules or carbon–water complexes. However, the strong difference in friction between D_2O and H_2O cannot be attributed to sample contaminations, because the sample preparations were

https://doi.org/10.1021/acs.nanolett.2c01425
Nano Lett. 2022, 22, 7761–7767

identical, and thus sample contamination densities should also be identical for D_2O and H_2O.

We assume that both D_2O and H_2O do not modify the mica surface. Thus, strain in graphene pieces can relax due to either sliding of the pieces on top of the lubricating films or strain relaxation within the lubricating films. The second scenario implies a drastic structural difference of the confined H_2O and D_2O films, which we assume not to be the case due to a known structural similarity of the bulk and of nanoconfined D_2O and H_2O.[26,27] Moreover, it implies that the difference in lubricities should not depend on graphene thickness, which contradicts our experimental findings. Even more, we expect ionic mica to strongly interact with the polar H_2O and D_2O molecules. Therefore, we assume graphene sliding on top of the lubricating film.

It has been experimentally shown using scanning force microscopy that hydrogen (H) passivated surfaces exhibited approximately 30% higher friction applied to an AFM tip sliding the surface to compare with deuterium (D) passivated ones.[28] The differences were attributed to the difference in vibrational frequencies of H and D adsorbates colliding with the sliding surfaces at different rates, which determine different rates of conversion of kinetic energy into heat. Even if water molecules became perfectly oriented by the ionic mica surface with H (or D) pointing toward graphene, one might expect only about 30% higher friction on H_2O film compared to D_2O film, following the arguments in ref 28. That is, the mechanism does not allow to explain the giant difference in the lubricities we observe. Moreover, the mechanism was questioned by the argument that the smaller momentum transfer by the lighter hydrogen per vibrational cycle overcompensates for the faster collision rates.[29] Another possibly contributing phenomenon may be the difference in the overlaps of the phonon spectra of graphene and mica with vibrational modes of the lubricating molecules. From this, however, it is difficult to predict an order of magnitude difference in friction.[30] Moreover, it does not allow us to explain why the exceptionally poor lubricity of the H_2O film is limited to SLG. A different, recently proposed friction mechanism due to quantum fluctuations leads to friction growing with the thickness of graphene,[5] which here is not the case.

We propose that the anomalously poor lubricity of H_2O films at the single-layer graphene−mica interface is related to the high permeability of single-layer graphene to protons. Graphene is well permeable to protons, but is at least an order of magnitude less permeable for deuterons.[31,32] Moreover, both protons and deuterons hardly permeate double-layer graphenes. We assume that protons permeating through graphene form electrostatically bound ion pairs with the hydroxides remaining on the other side of graphene (Figure 2D). We propose furthermore that the ion pairs clamped across graphene effectively anchor the graphene in the water layer and hence reduce the lubricity and slow down the strain relaxation.

The proposed formation of ion pairs clamped across the graphene layer is expected to affect also other properties of the confined H_2O on the interface. Since the hydroxides are embedded in the water film, the diffusion of the water molecules around them should be hindered, and the effective coefficient of self-diffusion should be lower, while the corresponding effective viscosity should be higher. Further indication for a huge difference in this effective viscosity is obtained from the behavior of the filling (draining) of the graphene−mica slit pore, a process we refer to as wetting (dewetting). Both, wetting and dewetting of the graphene-mica interface with H_2O has been detailed previously[33] (see also the Supporting Information for a detailed experimental description). Since liquid must enter (exit) from the boundary of the graphene flakes, transport of liquid within the graphene−mica slit pore is essential during wetting (dewetting), and hence the effective viscosity of the system must play a role in this process. In ref 33 the wetting (dewetting) was initiated by a change of relative humidity (RH) of the environment, and then the graphene layer imaged over time with atomic force microscopy (AFM) (see the Supporting Information for more details). Here, the same experiments were performed with graphene flakes on mica using either H_2O or D_2O vapor.

In the case of wetting, typical patterns are very similar for H_2O and D_2O, see the Supporting Information. The water layer creeps from the edges under the graphene and forms finger-like structures that evolve into a labyrinthine pattern representing a structure close to equilibrium.[33] The evolution of this pattern is very slow and can hardly be affected by the values of effective viscosity. At high humidities, the water film closes to form a homogeneous layer.

In the case of dewetting, in contrast, we find different patterns for H_2O and D_2O films, if the humidity conditions are selected properly. Here the patterns are due to the dry phase, i.e. graphene directly attached to the mica with the water layer removed (marked blue in Figure 3). If RH is reduced from originally 40% by purging the measurement chamber with nitrogen to almost 0% ("fast dewetting"), both films, H_2O and D_2O, produce very similar ramified fractal patterns with fractal dimensions of 1.7 (see the Supporting Information). However, if the RH is decreased moderately from originally 40% to about 13% ("slow dewetting"), we observe a strong difference in the dewetting patterns. Only the patterns of SLG on H_2O are ramified with dimension 1.7 (Figure 3A), while the patterns of SLG on D_2O are much more compact (Figure 3B). Also bi- and multilayer graphene on H_2O or D_2O show very compact dewetting patterns (see Figure 3C, D).

The fractal growth of the dry phase during dewetting was attributed to diffusion limited aggregation (DLA),[33] to viscous fingering,[34] or even to water crystal growth.[35] However, regardless of the description of the mechanism, the dewetted phase has to grow at the cost of displacement of the liquid phase and critically depends on its effective viscosity. In experiments on viscous fingering, a phase with low viscosity is growing into a phase of higher viscosity.[36] In two-dimensional lipid monolayers,[37] the growth is limited by the diffusion of impurities within the liquid phase and hence corresponds to diffusion-limited aggregation. In both cases, however, the pattern becomes more ramified the larger the viscosity of the outer phase or the faster and higher the jump in external driving force (difference in RH in our case). Here, in the case of *fast* dewetting, the humidity jump is fast enough for the given effective viscosities of both H_2O and D_2O to cause growth of ramified fractals. For the *slow* dewetting, a difference in effective viscosity becomes apparent, see Figure 3. It was shown by numerical simulations as well as by experiments,[36] that under otherwise comparable conditions, the viscosity of the outer phase must vary by orders of magnitude, in order to induce changes in the morphology and hence fractal dimensions as observed here. Therefore, we consider the observed difference in dewetting structures for H_2O and D_2O as a further indication of a giant increase in the effective

https://doi.org/10.1021/acs.nanolett.2c01425
Nano Lett. 2022, 22, 7761−7767

viscosity of the H_2O compared to the D_2O film. The finding of similar dewetting patterns for D_2O and H_2O below multilayer graphene (Figure 3) indicates lower effective viscosity. Hence, the dewetting experiments confirm that the giant effective viscosity (connected with poor lubricity) is an outstanding property of the single-layer graphene−H_2O−mica system.

In conclusion, we demonstrate that H_2O films confined at a single-layer graphene−mica interface show at least an order of magnitude worse lubricity compared with D_2O films at the same interface and compared with H_2O films at a double-layer graphene−mica interface. The poor lubricity of the H_2O film is limited to graphene monolayers. Therefore, the effect we report is important for understanding of the lubricity of surfaces coated with single-layer graphene but has probably a limited impact on H_2O lubrication of bulk graphite. The results of strain relaxation experiments are confirmed by the ones for dewetting kinetics of the molecular films confined at the interfaces, which can be explained by the higher effective viscosity of water in a mica−H_2O−graphene system.

We propose a model that qualitatively explains the poor lubricity of the H_2O film, or the high effective viscosity of the graphene H_2O system, by the permeability of single-layer graphene to protons. This permeability allows proton-hydroxide ion pairs to form complexes separated by graphene. These ion pairs are fixed with respect to lateral movement and hence present a solid obstacle to the flow of the surrounding water layer. Lower permeability of deuterons through graphene then results in lower concentrations of the ion pairs, allowing for faster graphene sliding.

The proposed difference in the ion pair concentrations hindering single-layer graphene sliding might further affect properties of graphene monolayers exfoliated onto substrates. We expect the ion pairs to increase adhesion and thus reduce buckling of single-layer graphenes on hydrophilic substrates. Ion pairs might also add frictional forces to, for example, AFM friction experiments. Furthermore, the proposed ion pairs might also influence properties of bulk materials comprising single-layer graphenes or other aromatic carbon materials. For example, our work might contribute to the understanding of the lateral transport of water and heavy water through graphene oxide membranes and their selective permeation, which may be employed for water filtering.[38,39] Furthermore, similar phenomena can be expected for other proton-selective 2D materials like hexagonal boron nitride.

■ ASSOCIATED CONTENT

Supporting Information

The Supporting Information is available free of charge at https://pubs.acs.org/doi/10.1021/acs.nanolett.2c01425.

Materials and methods, slow wetting and dewetting, fast dewetting, single-layer and bilayer graphenes after strain measurements, strain relaxations for H_2O and D_2O mixtures (Figures S1−S10) (PDF)

■ AUTHOR INFORMATION

Corresponding Author

Jürgen P. Rabe − *Department of Physics & IRIS Adlershof, Humboldt-Universität zu Berlin, Berlin 12489, Germany;* orcid.org/0000-0003-0847-6663; Email: rabe@hu-berlin.de

Authors

Hu Lin − *Department of Physics & IRIS Adlershof, Humboldt-Universität zu Berlin, Berlin 12489, Germany;* orcid.org/0000-0003-3382-720X

Lala Habibova − *Department of Physics & IRIS Adlershof, Humboldt-Universität zu Berlin, Berlin 12489, Germany*

Abdul Rauf − *Department of Physics & IRIS Adlershof, Humboldt-Universität zu Berlin, Berlin 12489, Germany*

José D. Cojal González − *Department of Physics & IRIS Adlershof, Humboldt-Universität zu Berlin, Berlin 12489, Germany*

Nikolai Severin − *Department of Physics & IRIS Adlershof, Humboldt-Universität zu Berlin, Berlin 12489, Germany;* orcid.org/0000-0001-7007-7124

Stefan Kirstein − *Department of Physics & IRIS Adlershof, Humboldt-Universität zu Berlin, Berlin 12489, Germany;* orcid.org/0000-0002-4608-8410

Igor M. Sokolov − *Department of Physics & IRIS Adlershof, Humboldt-Universität zu Berlin, Berlin 12489, Germany*

Complete contact information is available at: https://pubs.acs.org/10.1021/acs.nanolett.2c01425

Notes

The authors declare no competing financial interest.

■ ACKNOWLEDGMENTS

This work was supported by Deutsche Forschungsgemeinschaft (Projektnummer 182087777-SFB 951, S.K. and J.P.R.) and the Cluster of Excellence "Matters of Activity. Image Space Material" under Germany's Excellence Strategy EXC 2025 (J.D.C.G. and J.P.R.).

■ REFERENCES

(1) Klein, J. Hydration lubrication. *Friction* **2013**, *1* (1), 1−23.

(2) Ikari, M. J.; Saffer, D. M.; Marone, C. Effect of hydration state on the frictional properties of montmorillonite-based fault gouge. *Journal of Geophysical Research: Solid Earth* **2007**, *112* (6), B06423.

(3) Savage, R. H. Graphite lubrication. *J. Appl. Phys.* **1948**, *19* (1), 1−10.

(4) Faucher, S.; Aluru, N.; Bazant, M. Z.; Blankschtein, D.; Brozena, A. H.; Cumings, J.; Pedro De Souza, J.; Elimelech, M.; Epsztein, R.; Fourkas, J. T.; et al. Critical Knowledge Gaps in Mass Transport through Single-Digit Nanopores: A Review and Perspective. *J. Phys. Chem. C* **2019**, *123* (35), 21309−21326.

(5) Kavokine, N.; Bocquet, M. L.; Bocquet, L. Fluctuation-induced quantum friction in nanoscale water flows. *Nature* **2022**, *602* (7895), 84−90.

(6) Dai, Z.; Lu, N.; Liechti, K. M.; Huang, R. Mechanics at the interfaces of 2D materials: Challenges and opportunities. *Curr. Opin. Solid State Mater. Sci.* **2020**, *24* (4), 100837.

(7) Christenson, H. K.; Thomson, N. H. The nature of the air-cleaved mica surface. *Surf. Sci. Rep.* **2016**, *71* (2), 367−390.

(8) Israelachvili, J.; Min, Y.; Akbulut, M.; Alig, A.; Carver, G.; Greene, W.; Kristiansen, K.; Meyer, E.; Pesika, N.; Rosenberg, K.; et al. Recent advances in the surface forces apparatus (SFA) technique. *Rep. Prog. Phys.* **2010**, *73* (3), 036601.

(9) Lin, H.; Schilo, A.; Kamoka, A. R.; Severin, N.; Sokolov, I. M.; Rabe, J. P. Insight into the wetting of a graphene-mica slit pore with a monolayer of water. *Phys. Rev. B* **2017**, *95* (19), 195414.

(10) Rauf, A.; Cojal González, J. D.; Balkan, A.; Severin, N.; Sokolov, I. M.; Rabe, J. P. Shaping surfaces and interfaces of 2D materials on mica with intercalating water and ethanol. *Mol. Phys.* **2021**, *119* (15−16), e1947534.

(11) Gong, L.; Kinloch, I. A.; Young, R. J.; Riaz, I.; Jalil, R.; Novoselov, K. S. Interfacial stress transfer in a graphene monolayer nanocomposite. *Adv. Mater.* **2010**, *22* (24), 2694−2697.
(12) Dai, Z.; Wang, G.; Liu, L.; Hou, Y.; Wei, Y.; Zhang, Z. Mechanical behavior and properties of hydrogen bonded graphene/polymer nano-interfaces. *Compos. Sci. Technol.* **2016**, *136*, 1−9.
(13) Lin, H.; Rauf, A.; Severin, N.; Sokolov, I. M.; Rabe, J. P. Influence of interface hydration on sliding of graphene and molybdenum-disulfide single-layers. *J. Colloid Interface Sci.* **2019**, *540*, 142−147.
(14) Mohiuddin, T. M. G.; Lombardo, A.; Nair, R. R.; Bonetti, A.; Savini, G.; Jalil, R.; Bonini, N.; Basko, D. M.; Galiotis, C.; Marzari, N.; et al. Uniaxial strain in graphene by Raman spectroscopy: G peak splitting, Grüneisen parameters, and sample orientation. *Physical Review B - Condensed Matter and Materials Physics* **2009**, *79* (20), 205433.
(15) Hardy, R. C.; Cottington, R. L. Viscosity of Deuterium Oxide and Water from 5° to 125°C. *J. Chem. Phys.* **1949**, *17* (5), 509−510.
(16) Lee, J. E.; Ahn, G.; Shim, J.; Lee, Y. S.; Ryu, S. Optical separation of mechanical strain from charge doping in graphene. *Nat. Commun.* **2012**, *3*, 1024.
(17) Shim, J.; Lui, C. H.; Ko, T. Y.; Yu, Y. J.; Kim, P.; Heinz, T. F.; Ryu, S. Water-gated charge doping of graphene induced by mica substrates. *Nano Lett.* **2012**, *12* (2), 648−654.
(18) Clough, S. A.; Beers, Y.; Klein, G. P.; Rothman, L. S. Dipole moment of water from Stark measurements of H2 2O, HDO, and D2O. *J. Chem. Phys.* **1973**, *59*, 2254−2259.
(19) Soper, A. K.; Benmore, C. J. Quantum differences between heavy and light water. *Phys. Rev. Lett.* **2008**, *101* (6), 065502.
(20) Lin, H.; Cojal González, J. D.; Severin, N.; Sokolov, I. M.; Rabe, J. P. Reversible Switching of Charge Transfer at the Graphene-Mica Interface with Intercalating Molecules. *ACS Nano* **2020**, *14* (9), 11594−11604.
(21) Sgouros, A. P.; Androulidakis, C.; Tsoukleri, G.; Kalosakas, G.; Delikoukos, N.; Signetti, S.; Pugno, N. M.; Parthenios, J.; Galiotis, C.; Papagelis, K. Efficient Mechanical Stress Transfer in Multilayer Graphene with a Ladder-like Architecture. *ACS Appl. Mater. Interfaces* **2021**, *13* (3), 4473−4484.
(22) Edgeworth, R.; Dalton, B. J.; Parnell, T. The pitch drop experiment. *Eur. J. Phys.* **1984**, *5* (4), 198−200.
(23) Rezania, B.; Dorn, M.; Severin, N.; Rabe, J. P. Influence of graphene exfoliation on the properties of water-containing adlayers visualized by graphenes and scanning force microscopy. *J. Colloid Interface Sci.* **2013**, *407*, 500−504.
(24) Dowsett, M. G.; King, R. M.; Parker, E. H. C. Evaluation of impurity and contamination levels on mica surfaces using SSIMS. *J. Vac. Sci. Technol.* **1977**, *14* (2), 711−717.
(25) Poppa, H.; Elliot, A. G. The surface composition of Mica substrates. *Surf. Sci.* **1971**, *24* (1), 149−163.
(26) Shrestha, B. R.; Pillai, S.; Santana, A.; Donaldson, S. H.; Pascal, T. A.; Mishra, H. Nuclear Quantum Effects in Hydrophobic Nanoconfinement. *J. Phys. Chem. Lett.* **2019**, *10* (18), 5530−5535.
(27) Ceriotti, M.; Fang, W.; Kusalik, P. G.; McKenzie, R. H.; Michaelides, A.; Morales, M. A.; Markland, T. E. Nuclear Quantum Effects in Water and Aqueous Systems: Experiment, Theory, and Current Challenges. *Chem. Rev.* **2016**, *116* (13), 7529−7550.
(28) Cannara, R. J.; Brukman, M. J.; Cimatu, K.; Sumant, A. V.; Baldelli, S.; Carpick, R. W. Nanoscale friction varied by isotopic shifting of surface vibrational frequencies. *Science* **2007**, *318* (5851), 780−783.
(29) Mo, Y.; Müser, M. H.; Szlufarska, I. Origin of the isotope effect on solid friction. *Physical Review B - Condensed Matter and Materials Physics* **2009**, *80* (15), 155438.
(30) Lee, H.; Ko, J. H.; Song, H. C.; Salmeron, M.; Kim, Y. H.; Park, J. Y. Isotope- and Thickness-Dependent Friction of Water Layers Intercalated Between Graphene and Mica. *Tribol. Lett.* **2018**, *66* (1), 36.
(31) Lozada-Hidalgo, M.; Hu, S.; Marshall, O.; Mishchenko, A.; Grigorenko, A. N.; Dryfe, R. A. W.; Radha, B.; Grigorieva, I. V.; Geim, A. K. Sieving hydrogen isotopes through two-dimensional crystals. *Science* **2016**, *351* (6268), 68−70.
(32) Bukola, S.; Liang, Y.; Korzeniewski, C.; Harris, J.; Creager, S. Selective Proton/Deuteron Transport through Nafion|Graphene|Nafion Sandwich Structures at High Current Density. *J. Am. Chem. Soc.* **2018**, *140* (5), 1743−1752.
(33) Rauf, A.; Schilo, A.; Severin, N.; Sokolov, I. M.; Rabe, J. P. Non-monotonous Wetting of Graphene-Mica and MoS2-Mica Interfaces with a Molecular Layer of Water. *Langmuir* **2018**, *34* (50), 15228−15237.
(34) Severin, N.; Lange, P.; Sokolov, I. M.; Rabe, J. P. Reversible dewetting of a molecularly thin fluid water film in a soft graphene-mica slit pore. *Nano Lett.* **2012**, *12* (2), 774−779.
(35) Bampoulis, P.; Siekman, M. H.; Kooij, E. S.; Lohse, D.; Zandvliet, H. J. W.; Poelsema, B. Latent heat induced rotation limited aggregation in 2D ice nanocrystals. *J. Chem. Phys.* **2015**, *143* (3), 034702.
(36) Zhang, J. H.; Liu, Z. H. Study of the relationship between fractal dimension and viscosity ratio for viscous fingering with a modified DLA model. *J. Pet. Sci. Eng.* **1998**, *21* (1−2), 123−128.
(37) Möhwald, H.; Göbel, H. D.; Flörsheimer, M.; Miller, A. Interfacial Instabilities of Condensed Phase Domains in Lipid Monolayers. In *Random Fluctuations and Pattern Growth: Experiments and Models*, Stanley, H. E., Ostrowsky, N., Eds.; Springer, 1988; pp 101−109.
(38) Mohammadi, A.; Daymond, M. R.; Docoslis, A. Graphene oxide membranes for isotopic water mixture filtration: Preparation, physicochemical characterization, and performance assessment. *ACS Appl. Mater. Interfaces* **2020**, *12* (31), 34736−34745.
(39) Ching, K.; Baker, A.; Tanaka, R.; Zhao, T.; Su, Z.; Ruoff, R. S.; Zhao, C.; Chen, X. Liquid-phase water isotope separation using graphene-oxide membranes. *Carbon* **2022**, *186*, 344−354.

https://doi.org/10.1021/acs.nanolett.2c01425
Nano Lett. 2022, 22, 7761−7767